The Berezinskii-Kosterlitz-Thouless Transition in the 2D XY Model

Lara Turgut, M.Sc. Physics
ETH Zurich, Zurich, Switzerland

Abstract
In this work, we investigate the Berezinskii–Kosterlitz–Thouless (BKT) transition in the two-dimensional classical XY model. Using the Wolff cluster algorithm, we simulate square lattices of sizes $L = \{20, 30, 40, 50, 60, 70\}$ over a temperature range $T \in [0.7, 1.5]$. We analyze thermodynamic observables, including the spin stiffness, spin–spin correlation function, and vortex density. The BKT transition temperature T_{BKT} is extracted from the universal jump in the spin stiffness Υ, the condition $\eta = 1/4$ for the exponent governing the algebraic decay of spin–spin correlations at criticality, and the exponential divergence of the correlation length ξ.We obtain $T_{\mathrm{BKT}}^{\Upsilon} \approx 0.8934 \pm 0.0024$, $T_{\mathrm{BKT}}^{\eta} \approx 0.8946 \pm 0.0022$, and $T_{\mathrm{BKT}}^{\xi} \approx 0.8098 \pm 0.0073$. The estimate from spin stiffness agrees well with the literature value $T_{\mathrm{BKT}}^{\mathrm{lit}} = 0.89213(10)$ [10]. The value obtained from η is in close agreement, while the estimate from ξ shows a more pronounced deviation, likely due to the sensitivity of the exponential fit and finite-size effects.

Contents

1 Introduction

The two-dimensional XY model describes a system of classical planar spins $\mathbf{S}_i = (\cos\theta_i, \sin\theta_i)$, where $\theta_i \in [0, 2\pi)$ is the angle of the spin at site i relative to a fixed axis. The Hamiltonian is given by

$$H = -J \sum_{\langle i,j \rangle} \mathbf{S}_i \cdot \mathbf{S}_j = -J \sum_{\langle i,j \rangle} \cos(\theta_i - \theta_j), \quad (1)$$

where the sum runs over all pairs of nearest-neighbor sites, and J is the coupling constant.

In the ferromagnetic case $J > 0$, the system minimizes its energy at zero temperature by aligning all spins in the same direction; that is, $\theta_i = \theta_0$ for all i, where $\theta_0 \in [0, 2\pi)$ is an arbitrary global angle. The selection of a specific angle θ_0 breaks the continuous $O(2)$ symmetry of the Hamiltonian spontaneously.*

At finite temperatures, the behavior of the system is constrained by the Mermin–Wagner theorem[7]:

> *In dimensions $d \leq 2$, a system with a continuous symmetry and short-range interactions cannot exhibit a stable long-range ordered state at finite temperature.*

As a result, in the two-dimensional XY model at any nonzero temperature $T > 0$, thermal fluctuations prevent the emergence of true long-range order.

Remarkably, the two-dimensional XY model exhibits a *topological* phase transition, known as the Berezinskii–Kosterlitz–Thouless (BKT) transition, which constitutes the focus of this work.

2 Theoretical Background[2]

2.1 BKT transition

In the late 1970s, Berezinskii, Kosterlitz, and Thouless demonstrated that the XY model exhibits *quasi-long-range order*(QLRO) at low temperatures and a disordered phase at high temperatures. This transition, known as the Berezinskii–Kosterlitz–Thouless (BKT) transition, is a topological phase transition and is of infinite order.

2.2 Spin-wave approximation

At low temperatures, the spins in the XY model are nearly aligned: $|\theta_i - \theta_j| \ll 2\pi$. In this regime, one can expand the cosine in the Hamiltonian in a Taylor series:

$$H \approx -JN + \frac{J}{2} \sum_{\langle i,j \rangle} (\theta_i - \theta_j)^2,$$

where N is the number of spins. Rewriting the sum over pairs $\langle i, j \rangle$ as a sum over lattice sites $\mathbf{r}$ and their nearest neighbors $\mathbf{r} + \mathbf{a}$, this becomes

$$H = E_0 + \frac{J}{4} \sum_{r,a} \left(\theta(\mathbf{r} + \mathbf{a}) - \theta(\mathbf{r})\right)^2,$$

where $E_0 = -JN$ is a constant. In the continuum limit, the discrete differences become spatial derivatives, and the sum becomes an integral. The Hamiltonian then takes the form

$$H \simeq E_0 + \frac{J}{2} \int d^2r \, (\nabla\theta(\mathbf{r}))^2. \quad (2)$$

2.3 Correlation Functions

The spin–spin correlation function is defined as

$$g(r) = \langle e^{i(\theta(\mathbf{r}) - \theta(0))} \rangle, \quad (3)$$

where $\theta(\mathbf{r})$ denotes the angle of the spin at position $\mathbf{r}$.

By decomposing $\theta(\mathbf{r})$ into its Fourier modes,

$$\theta(\mathbf{r}) = \sum_{\mathbf{k}} \theta_{\mathbf{k}} \, e^{i\mathbf{k}\cdot\mathbf{r}},$$

and substituting this into the spin-wave Hamiltonian (7), one can derive the behavior of the correlation function (3) in the low-temperature regime. In this limit, the system

*Spontaneous symmetry breaking occurs when the Hamiltonian is symmetric under a transformation, but the statistical state of the system does not exhibit that symmetry.

exhibits *quasi-long-range order* (QLRO), and the correlation function decays algebraically:

$$g(r) \sim r^{-\eta(T)}, \tag{4}$$

where $\eta(T)$ is a temperature-dependent exponent.

In the high-temperature regime, the behavior of $g(r)$ can be obtained via a high-temperature expansion of the partition function. The system enters a disordered phase, and the correlation function decays exponentially:

$$g(r) \sim e^{-r/\xi(T)}, \tag{5}$$

with a finite correlation length $\xi(T)$. In contrast, in the low-temperature phase, the correlation length is infinite, $\xi = \infty$, indicating that the system is scale-free in this regime.

2.4 Vortices and Antivortices

Vortices are topological defects of the field $\theta(\mathbf{r})$, which satisfies the Laplace equation $\nabla^2\theta(\mathbf{r}) = 0$ in the absence of sources. In addition to the trivial solution $\theta(\mathbf{r}) = \text{const}$, there exist nontrivial solutions: vortices. For a single vortex located at $\mathbf{r}_0$, the circulation of the gradient of θ around a closed loop γ enclosing the defect is quantized:

$$\oint_\gamma \nabla\theta(\mathbf{r}) \cdot d\mathbf{l} = 2\pi n, \tag{6}$$

where $n \in \mathbb{Z}$ is the topological charge or winding number of the vortex. A positive n corresponds to a vortex, while a negative n describes an antivortex.

The energy of a single vortex in the XY model scales logarithmically with system size as $\Delta E = \pi J n^2 \ln(L/a)$, where L is the system size and a is the lattice spacing. The associated entropy gain from placing a vortex anywhere in the system is $\Delta S = 2k_B \ln(L/a)$, leading to a free energy cost of

$$\Delta F = \Delta E - T\Delta S = (\pi J n^2 - 2k_B T)\ln(L/a).$$

This expression reveals a crucial insight: for temperatures below the $T_c = \frac{\pi J n^2}{2k_B}$, the free energy cost of creating a free vortex is positive, so vortices remain bound in vortex–antivortex pairs. For $T > T_c$, the free energy becomes negative, allowing free vortices to proliferate. This unbinding drives the BKT transition.

While the free energy estimate for the BKT transition temperature provides an insight, it is only a crude estimation.

In contrast, the free energy of a vortex–antivortex pair separated by a distance r is given by

$$\Delta F_{\text{pair}} = (\pi J - 2k_B T)\ln\left(\frac{r}{a}\right),$$

which does not diverge with system size like the free energy of a single vortex. Instead, it remains finite for finite r, making vortex pairs energetically favorable at low temperatures.

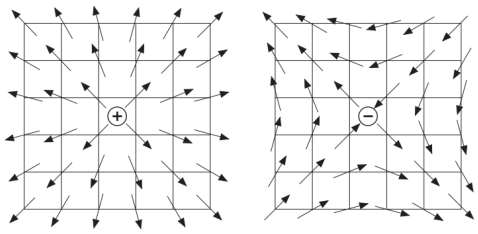

Figure 1: The two elementary vortices in the XY model.[3]

2.5 Renormalization Group

The renormalization group (RG) framework will not be discussed in detail; instead, a brief insight into its relevance for the BKT transition will be provided.

A more detailed treatment of the BKT transition involves a renormalization group (RG) analysis.

To start with the renormalization group (RG) analysis, it is useful to map the partition function of the 2D classical XY model to that of a 2D Coulomb gas.

When electromagnetic interactions are strictly confined in two dimensions, the Coulomb interaction between two charges no longer behaves as $q_1 q_2/r$, but instead as $q_1 q_2 \log(r)$, where r is the separation between the charges. Remarkably, this effective interaction arises

naturally from the 2D XY model when vortices are taken into account.

2.5.1 Mapping to the Coulomb gas [2] [8]

We start from the spin–wave approximation, valid at low temperatures (ignoring the constant term):

$$H = \frac{J}{2} \int d^2r \, (\nabla\theta(\mathbf{r}))^2. \tag{7}$$

While this approximation captures smooth fluctuations of $\theta(\mathbf{r})$, it does not account for vortices. To incorporate vortices into this framework, we recall the condition that defines their presence in Eq. (6).

It is useful to separate the two contributions to the fluctuations of the XY model: spin waves and vortices. We decompose $\mathbf{u} = \nabla\theta(\mathbf{r})$ into two components: $\mathbf{u} = \mathbf{u}_0 + \mathbf{u}_v$, where $\mathbf{u}_0 = \nabla\phi$ is the spin waves, and $\mathbf{u}_v$ captures vortices. Using the circulation condition around a vortex of charge n in Eq. (6), the vorticity is given by

$$\nabla \times \mathbf{u} = 2\pi\hat{z} \sum_j n_j \delta(\mathbf{r} - \mathbf{r}_j),$$

where $n_j \in \mathbb{Z}$ is the winding number of a vortex at position $\mathbf{r}_j$.

To satisfy this vorticity condition, we express the vortex part of the field as $\mathbf{u}_v = -\nabla\times(\hat{z}\psi)$, leading to the decomposition

$$\mathbf{u} = \nabla\phi - \nabla \times (\hat{z}\psi). \tag{8}$$

Taking the curl of both sides of the velocity field decomposition and applying standard vector identities, we obtain a Poisson equation for the scalar field ψ:

$$\nabla^2\psi = 2\pi \sum_j n_j \delta(\mathbf{r} - \mathbf{r}_j),$$

which corresponds to the electrostatic potential generated by point charges n_j located at positions $\mathbf{r}_j$ in two dimensions. The solution to this equation is

$$\psi(\mathbf{r}) = \sum_j n_j \ln|\mathbf{r} - \mathbf{r}_j|,$$

demonstrating that the vortex contribution behaves like a logarithmic potential in 2D, analogous to the interaction between electric charges in a Coulomb gas.

Substituting the decomposition (8) into the spin-wave Hamiltonian (7), we find that the total energy separates into a spin-wave term and a vortex–vortex interaction term:

$$H\left(\phi(\mathbf{r}), \{n_i, \mathbf{r}_i\}\right) = H_0\left(\phi(\mathbf{r})\right) + H_1\left(\{n_i, \mathbf{r}_i\}\right),$$

$$H_0 = \frac{J}{2} \int |\nabla\phi(\mathbf{r})|^2 \, d^2r,$$

$$H_1 = -\sum_i \varepsilon(n_i) - J\pi \sum_{i,j} n_i n_j \ln\left(|\mathbf{r}_i - \mathbf{r}_j|\right)$$

where H_0 accounts for smooth spin-wave fluctuations, and H_1 captures the pairwise interaction energy between vortices. The first term in H_1 accounts for the core energy of the vortices. We consider only the most probable excitations with $n_i = \pm 1$.

Accordingly, the partition function can be factorized as

$$Z = Z_{\text{sw}} \cdot Z_{\text{vortex}},$$

where the spin-wave contribution is given by a Gaussian integral over smooth configurations,

$$Z_{\text{sw}} = \int \mathcal{D}\phi \, e^{-\beta H_0[\phi]},$$

and the vortex contribution becomes a grand-canonical partition function [3] over all possible vortex configurations:

$$Z_{\text{vortex}} = \sum_{N=0}^{\infty} y_0^N \int \left(\prod_{i=1}^{N} d^2\mathbf{r}_i\right) \times \exp\left(2K\pi \sum_{i<j} n_i n_j \ln\left(|\mathbf{r}_i - \mathbf{r}_j|\right)\right)$$

where $y_0 = e^{-\beta\varepsilon}$ is the vortex fugacity, a is the lattice spacing, $K = \beta J$ and the sum runs over neutral configurations of N vortices and N antivortices (i.e., $\sum_i n_i = 0$). This representation reveals the equivalence between the vortices of the XY model and a 2D Coulomb gas.

2.5.2 RG flow equations

In this section, the RG flow equations for the 2D Coulomb gas are presented. For a detailed derivation, please refer to [2] [3].

Effective Interaction. The interaction between two charges located at positions $\mathbf{r}$ and $\mathbf{r}'$ becomes screened by the surrounding vortex–antivortex pairs. This screening modifies the bare interaction and results in an effective interaction described by the effective Hamiltonian:

$$\mathcal{H}_{\text{eff}}(\mathbf{r}-\mathbf{r}') = -2\pi K_{\text{eff}} \ln|\mathbf{r}-\mathbf{r}'|,$$

where $\mathcal{H}_{\text{eff}} = -\beta H_{\text{eff}}$, and K_{eff} is the renormalized, scale-dependent coupling constant. This expression reflects the influence of vortex–antivortex fluctuations on the effective interaction between test charges in the Coulomb gas representation.

A detailed calculation[2] shows that screening reduces the coupling:

$$K_{\text{eff}} = K - 4\pi^3 K^2 y_0^2 \int_1^R dx\, x^{3-2\pi K} + \mathcal{O}(y_0^4).$$

RG Flow Equations From the scale dependence of K and y_0, the following flow equations are derived:

$$\frac{dK^{-1}}{dl} = 4\pi^3 y_0^2 + \mathcal{O}(y_0^4),$$
$$\frac{dy_0}{dl} = (2-\pi K)y_0 + \mathcal{O}(y_0^3),$$

where l is a lengthscale over which we view our system. At $l = a$ the system is described by the bare parameters $K = J/T$ and $\epsilon = J\pi^2/2$ [6]. Note that $K_{\text{eff}} = \lim_{\ell\to\infty} K(\ell)$ and see the Fig. 2 for RG flow visualization.

Physical Interpretation

- For $\pi K > 2$ (low temperature), the vortex fugacity y_0 flows to zero, indicating that vortex–antivortex pairs remain tightly bound. The system exhibits quasi-long-range order.
- For $\pi K < 2$ (high temperature), the fugacity grows, leading to the unbinding and proliferation of free vortices. The system enters a disordered phase with exponentially decaying correlations.
- The critical point $\pi K_c = 2$ marks the BKT transition.

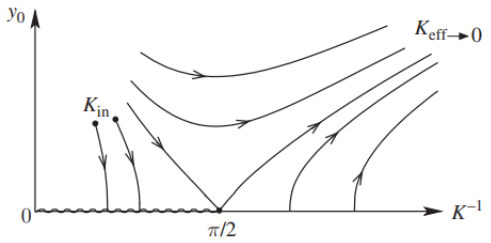

Figure 2: Renormalization group flows of the Coulomb gas system. [3]

2.5.3 Results from RG Flow Equations

The *spin stiffness* (or *helicity modulus*) Υ quantifies the system's resistance to a uniform twist in spin orientation. It is defined as the second derivative of the free energy $F(\phi)$ with respect to a small twist angle ϕ imposed via boundary conditions:

$$\Upsilon = \frac{1}{L^2}\frac{\partial^2 F(\phi)}{\partial \phi^2}\bigg|_{\phi=0},$$

where L is the system size. A nonzero Υ indicates quasi-long-range order, while $\Upsilon = 0$ corresponds to the disordered phase with free vortices. In simulations, Υ is computed via:

$$\Upsilon = \frac{J}{L^2}\left\langle \sum_{\langle i,j\rangle} \cos(\theta_i-\theta_j)(\hat{\mathbf{e}}_{ij}\cdot\hat{\mathbf{x}})^2 \right\rangle - \frac{J^2\beta}{L^2}\left\langle \left[\sum_{\langle i,j\rangle} \sin(\theta_i-\theta_j)(\hat{\mathbf{e}}_{ij}\cdot\hat{\mathbf{x}})\right]^2 \right\rangle,$$

where the sums run over all nearest-neighbor bonds, $\hat{\mathbf{e}}_{ij}$ is the unit vector from site i to site j, and the twist is applied in the x-direction. One could equally apply the twist in the y-direction; due to isotropy, the choice of direction does not affect the result. One can compute Υ separately in the x- and y-directions

and took their average to reduce finite-size effects.

A key prediction of BKT theory is the *Nelson–Kosterlitz universal jump*[9] in the helicity modulus at the transition temperature. As the system approaches T_{BKT} from below, the spin stiffness exhibits a discontinuous drop to zero:

$$\Upsilon(T_{\mathrm{BKT}}^{-}) = \frac{2k_B T_{\mathrm{BKT}}}{\pi}, \tag{9}$$

indicating the unbinding of vortex–antivortex pairs.

Another fundamental quantity in BKT theory is the *critical exponent* $\eta(T)$, which governs the algebraic decay of spin–spin correlations in the low-temperature phase:

$$g(r) = \langle \mathbf{S}(0) \cdot \mathbf{S}(r) \rangle \sim r^{-\eta(T)}.$$

At the transition temperature, one has:

$$\eta(T_{\mathrm{BKT}}) = \frac{1}{4} \quad [1]$$

Finally, the *correlation length* ξ in the disordered phase ($T > T_{\mathrm{BKT}}$) behaves like:

$$\xi(T) \approx a \exp\left[\frac{\pi^2}{8b}\sqrt{\frac{T_{\mathrm{BKT}}}{T - T_{\mathrm{BKT}}}}\right], \tag{10}$$

where a is the lattice spacing and b is a non-universal constant.

Hence, in contrast to conventional second-order phase transitions, standard observables such as the magnetization or susceptibility do not serve as reliable order parameters for identifying the BKT transition; instead, quantities like the spin stiffness Υ, the exponent η and correlation length ξ provide more direct signatures of the transition's topological nature.

2.6 Other Observables

In addition, we compute several other thermodynamic observables for further analysis. These include the energy per site e, magnetization per site m, specific heat c_v, magnetic susceptibility χ, and Binder cumulant U, defined as:

$$\begin{aligned}
e &= \frac{E}{N} = -\frac{J}{N}\left\langle \sum_{\langle i,j \rangle} \cos(\theta_i - \theta_j) \right\rangle, \\
m &= \frac{|\mathbf{M}|}{N} = \frac{1}{N}\left\langle \left| \sum_i \{\cos\theta_i, \sin\theta_i\} \right| \right\rangle, \\
c_v &= \frac{\langle E^2 \rangle - \langle E \rangle^2}{NT^2}, \\
\chi &= \frac{\langle |\mathbf{M}|^2 \rangle - \langle |\mathbf{M}| \rangle^2}{NT}, \\
U &= 1 - \frac{\langle |\mathbf{M}|^4 \rangle}{3\langle |\mathbf{M}|^2 \rangle^2}.
\end{aligned}$$

Topological defects are quantified via the vorticity $\omega_{\mathrm{v},\square}$ around an elementary plaquette $\square$, defined as

$$\omega_{\mathrm{v},\square} = \frac{1}{2\pi} \sum_{\langle ij \rangle \in \square} \nabla\theta_{ij},$$

where the sum runs over the four bonds of the plaquette, and $\nabla\theta_{ij} \in [-\pi, \pi]$ is the angle difference [†]. The total vortex–antivortex pair density is then given by

$$\omega_{\mathrm{v}} = \frac{1}{2N}\left\langle \sum_{\square} |\omega_{\mathrm{v},\square}| \right\rangle.$$

3 Monte Carlo methods & implementation details

Simulating the XY model near the BKT transition is challenging due to critical slowing down and the need for large lattices to avoid finite-size effects.

3.1 Metropolis algorithm

In the Metropolis algorithm for the XY model, a spin update changes the angle θ_i at site i to

[†] $\nabla\theta_{ij} = \theta_i - \theta_j - 2\pi$ if $\theta_i - \theta_j > \pi$, and to $\nabla\theta_{ij} = \theta_i - \theta_j + 2\pi$ if $\theta_i - \theta_j < -\pi$.

a new value θ_i'. The energy change is then given by

$$\Delta E = -J \sum_{\langle i,j \rangle} \left[\cos(\theta_i' - \theta_j) - \cos(\theta_i - \theta_j) \right].$$

The new configuration is then accepted with probability $P = \min(1, e^{-\beta \Delta E})$. However, this algorithm becomes inefficient near the BKT transition due to large correlation, resulting in critical slowing down.

3.2 Wolff algorithm

To overcome this, we implemented the Wolff cluster algorithm[2], which significantly reduces critical slowing down by updating clusters of spins collectively.

The Wolff algorithm begins by choosing a random reflection axis, represented by a unit vector $\mathbf{r}$. A random site is selected as the seed of the cluster. Neighboring spins are added to the cluster with probability

$$P_{\text{add}} = 1 - \exp\left[\min\left(0, 2\beta J (\mathbf{S}_i \cdot \mathbf{r})(\mathbf{S}_j \cdot \mathbf{r})\right)\right],$$

which favors the inclusion of aligned spins along $\mathbf{r}$. Once the cluster is complete, all spins in it are reflected with respect to the chosen axis.

3.3 Implementation details

The simulation code (`simulate.py`) uses the Wolff algorithm (optionally Metropolis) and employs Numba's just-in-time (JIT) compilation[5] for performance optimization. Moreover, the simulations for different temperatures and system sizes were distributed over multiple CPU cores.

3.4 Jackknife Resampling

While basic observables such as energy and magnetization allow straightforward error estimation using the standard error of the mean, quantities that depend (possibly nonlinearly) on expectation values require resampling methods like the jackknife for reliable uncertainty estimates. This is because standard error propagation can become inaccurate in the presence of nonlinear dependencies or correlations between observables.[11] ‡

Hence, we used jackknife resampling to estimate the uncertainties for the susceptibility, specific heat, Binder cumulant, vortex density, spin stiffness, algebraic decay exponent η, and correlation length ξ.

Procedure[13] Given a dataset of n observations $X = \{x_1, x_2, \ldots, x_n\}$, the jackknife proceeds as:

- Construct n leave-one-out subsamples: $X_{(i)} = X \setminus \{x_i\}$.
- Compute the estimator on each subsample: $\hat{\theta}_{(i)}$.
- Compute the jackknife estimate: $\hat{\theta}_{\text{jack}} = \frac{1}{n} \sum_{i=1}^{n} \hat{\theta}_{(i)}$.
- Estimate variance: $\text{Var}_{\text{jack}}(\hat{\theta}) = \frac{n-1}{n} \sum_{i=1}^{n} (\hat{\theta}_{(i)} - \hat{\theta}_{\text{jack}})^2$.

Special case: For the sample mean, one can show that the jackknife estimate is equal to the usual mean: $\hat{\mu}_{\text{jack}} = \frac{1}{n} \sum_{i=1}^{n} \hat{\mu}_{(i)} = \bar{x}$, where $\bar{x}$ is the ordinary sample mean.

3.5 Uncertainty in $T_{\text{BKT}}(L)$

The transition temperature T_{BKT} is estimated from the universal jump condition (9):

$$\Upsilon(T_{\text{BKT}}) = \frac{2T_{\text{BKT}}}{\pi} \quad (k_B = 1),$$

i.e., as the root of $f(T) = \Upsilon(T) - \frac{2T}{\pi} = 0$.

To estimate the uncertainty in T_{BKT}, we apply the standard formula for propagation of uncertainty [12]. For a function $y = f(x)$, where x has uncertainty σ_x, the uncertainty in y is given by $\sigma_y = \left|\frac{df}{dx}\right| \sigma_x$. If we instead consider $x = f^{-1}(y)$, and y has uncertainty σ_y, then the uncertainty in x is $\sigma_x = \left|\frac{dx}{dy}\right| \sigma_y = \left|\frac{1}{df/dx}\right| \sigma_y$. In our case, the uncertainty in $f(T)$ arises entirely from the uncertainty in the

‡For example, the Binder cumulant $U = 1 - \frac{\langle M^4 \rangle}{3\langle M^2 \rangle^2}$ depends nonlinearly on correlated observables.

measured spin stiffness $\Upsilon(T)$, since the function $\frac{2T}{\pi}$ is known exactly. Thus, $\sigma_f = \sigma_\Upsilon(T)$, and the uncertainty in T_{BKT} becomes $\sigma_{T_{\mathrm{BKT}}} = \left|\frac{1}{f'(T)}\right| \sigma_\Upsilon(T)$ evaluated at $T = T_{\mathrm{BKT}}$.

The procedure for the extraction of T_{BKT} from the decay exponent η is analogous.

The uncertainty in T_{BKT} extracted from the correlation length was obtained from the covariance matrix returned by the fit to (10).

3.6 Finite–size scaling

To extract T_{BKT} in the thermodynamic limit, we performed a finite-size scaling analysis using the relation

$$T_{\mathrm{BKT}}(L) = T_{\mathrm{BKT}}(\infty) + \frac{a}{(\ln L)^2},$$

where a is a non-universal constant. A weighted linear regression was applied to $T_{\mathrm{BKT}}(L)$ plotted against $1/(\log L)^2$, using the inverse variances of the estimated $T_{\mathrm{BKT}}(L)$ values as weights to account for their uncertainties.

4 Results

We simulate the two-dimensional XY model with $J = 1$ on a square lattice using the Wolff cluster algorithm for system sizes $L = \{20, 30, 40, 50, 60, 70\}$ over a temperature range $T \in [0.7, 1.5]$. See Fig. 3 for the visualization of the XY model.

Figure 4 presents several thermodynamic observables as a function of temperature, for different lattice sizes.

The energy increase monotonically as a function of temperature, consistent with the absence of a phase transition due to symmetry breaking. We observe that the specific heat does not diverge at any temperature, and we observe a bump around at $T \sim 1.0$, indicating the unbinding of pairs.

The magnetization remains always finite at all temperatures, but it is reduced for increasing L, as expected from Mermin-Wagner theorem.

We observe that vortex density is near zero at low temperature, and it starts to increase with temperature.

Below the BKT transition temperature T_{BKT}, the spin–spin correlation function decays algebraically, leading to a susceptibility that diverges with the system size L. As the temperature approaches T_{BKT} from above, the susceptibility diverges exponentially due to the divergence of the correlation length. [4]

Moreover, one can see that, unlike in second-order phase transitions, the Binder cumulant curves in the XY model do not cross at a fixed point, reflecting the infinite-order nature of the BKT transition.

In Figure 5, we show observables that characterize the topological BKT transition. The spin stiffness exhibits a universal jump at the transition temperature. The algebraic decay exponent $\eta(T)$, extracted from the spin–spin correlation function, varies continuously with temperature in the low-temperature phase and reaches the universal value $\eta = 1/4$ at the critical point. Additionally, the correlation length diverges as the system approaches the transition temperature from above.

Figure 6 presents a finite-size scaling analysis of the spin stiffness, the algebraic decay exponent η, and the correlation length ξ. From these analyses, we extract the thermodynamic-limit estimates: $T_{\mathrm{BKT}}^{\Upsilon} \approx 0.8934 \pm 0.0024$, $T_{\mathrm{BKT}}^{\eta} \approx 0.8946 \pm 0.0022$, and $T_{\mathrm{BKT}}^{\xi} \approx 0.8998 \pm 0.0073$.

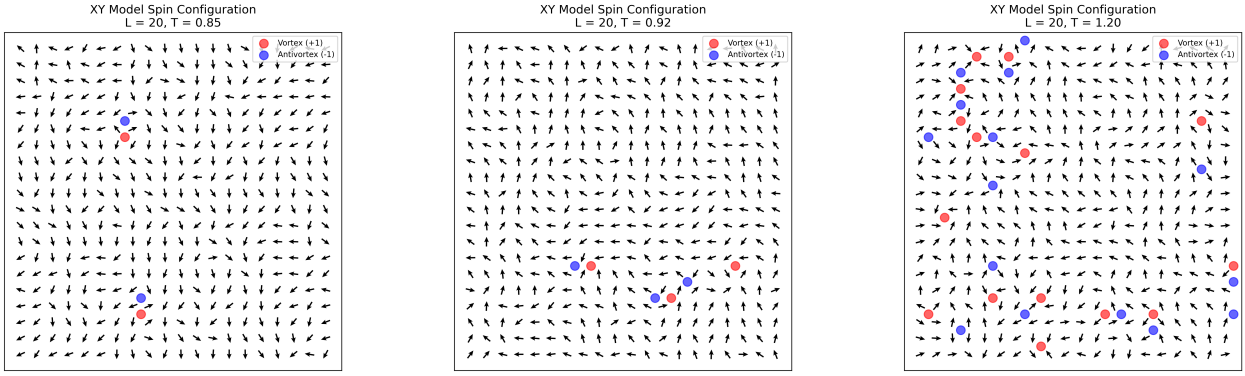

QLRO
$T = 0.85 \lesssim T_{\mathrm{BKT}}$

Transition
$T \approx 0.92 \gtrsim T_{\mathrm{BKT}}$

Disorder
$T = 1.20 > T_{\mathrm{BKT}}$

Figure 3: Configurations of the 2D XY model at different temperatures.

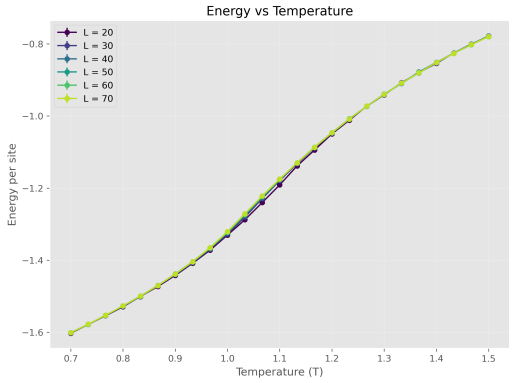

((a)) Energy

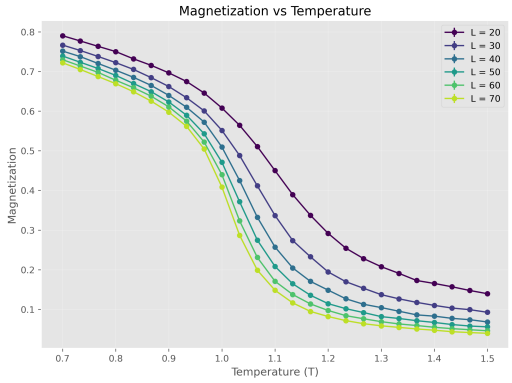

((b)) Magnetization

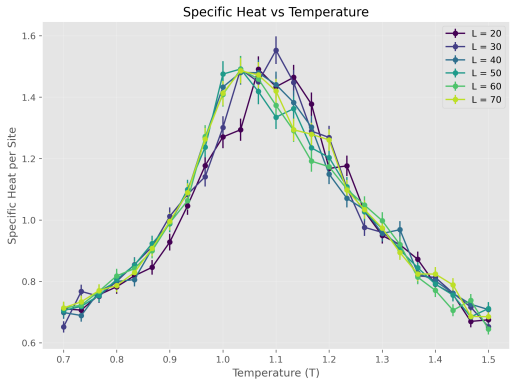

((c)) Specific heat

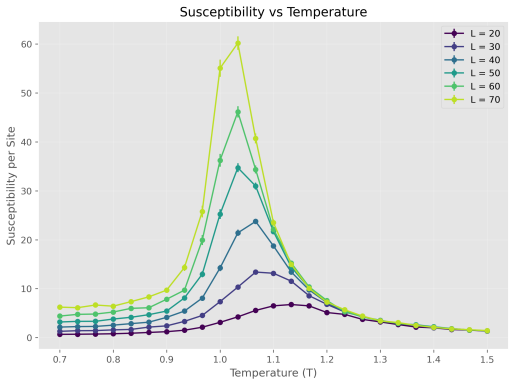

((d)) Susceptibility

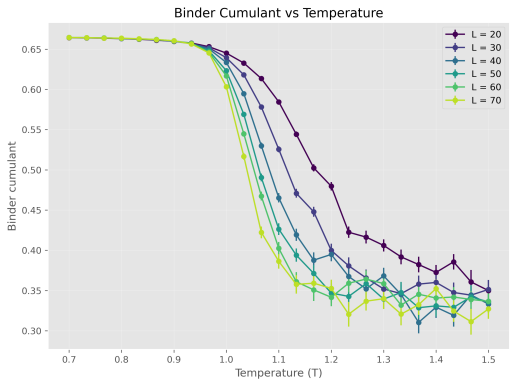

((e)) Binder cumulant

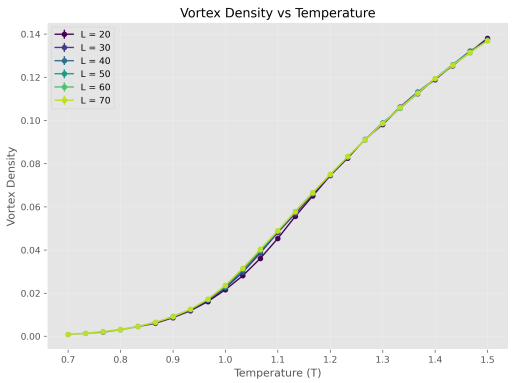

((f)) Vortex density

Figure 4: Results for the 2D classical XY model at different system sizes L, using the Wolff algorithm.

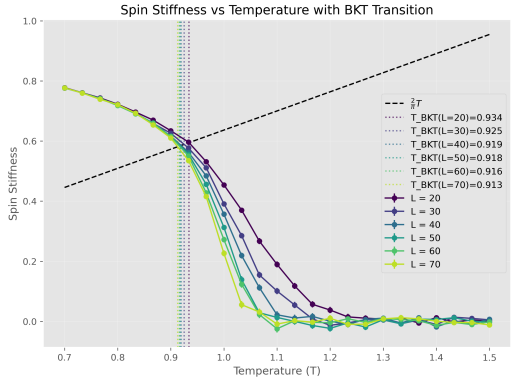

((a)) Spin stiffness

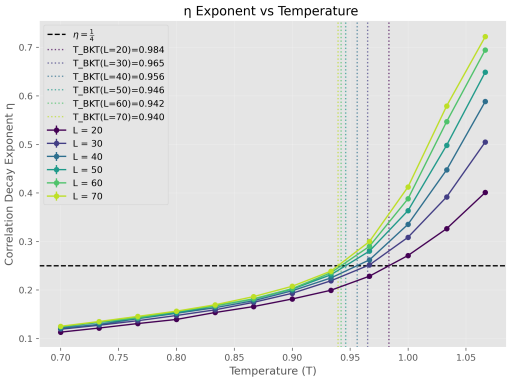

((b)) Algebraic decay exponent

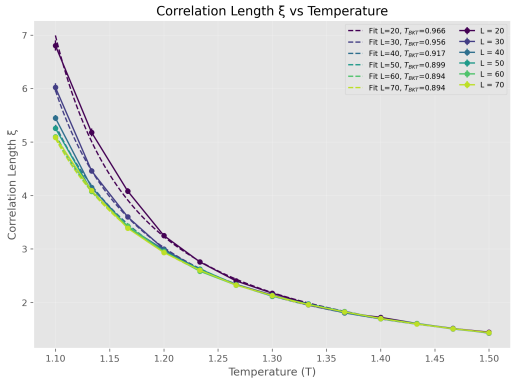

((c)) Correlation length

Figure 5: Results for the 2D classical XY model at different system sizes L, using the Wolff algorithm.

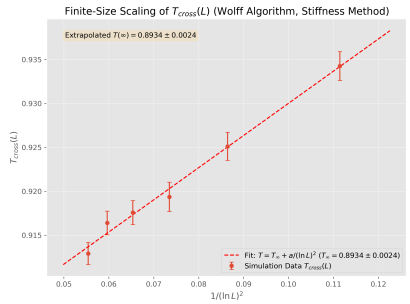

((a)) Spin stiffness

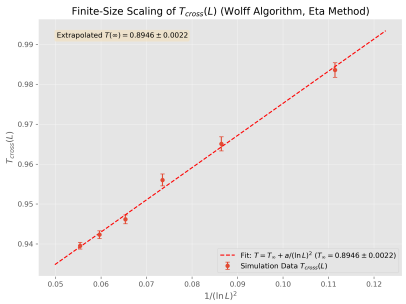

((b)) Exponent η

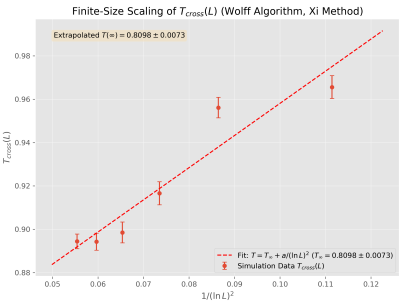

((c)) Correlation length ξ

Figure 6: Finite-size scaling analysis of the spin stiffness, algebraic decay exponent, and correlation length.

5 Discussion

Our results show the main features of the BKT transition, and the critical temperature extracted from the spin stiffness aligns well with the literature value. The critical temperature estimated from the algebraic decay exponent η differs slightly, likely due to finite-size effects and, limited number of sweeps and thermalization steps.

The estimate of T_{BKT} based on the correlation length ξ deviates more noticeably from the literature value. This is mainly because extracting T_{BKT} from $\xi(T)$ requires fitting the correlation length to an exponential function. However, this fit is highly sensitive to the number of temperature points close to T_{BKT},

where $\xi(T)$ grows rapidly. We repeated the simulations several times and found that the T_{BKT} estimate from ξ varied between runs, sometimes improving and sometimes worsening. We could also improve the simulations by using parallel tempering, which helps the system explore different states more efficiently. The performance could be improved by using parallel programming. Finally, the code could be written in a faster language like `C++`.

6 Conclusion

In this work, we investigated the BKT transition in the 2D classical XY model using the Wolff cluster algorithm. Our simulations reproduced the key features of the BKT transition, including the universal jump in the spin stiffness, the algebraic decay of correlations below the transition, and the exponential divergence of the correlation length above it.

We extracted the critical temperature T_{BKT} using three independent observables: the spin stiffness, the decay exponent η, and the correlation length ξ. The estimate from the spin stiffness showed agreement with the literature, while the result from η differed slightly, likely due to finite-size effects and limited statistics. The estimate from ξ showed the largest deviation, which we attribute to the sensitivity of the exponential fit and the sparse sampling of temperature points near the transition. Repeating the simulations showed that the ξ-based estimate varied noticeably between runs.

Overall, our findings confirm the topological nature of the BKT transition. Future improvements could include denser temperature sampling, longer simulations, and the use of parallel tempering to enhance state-space exploration. Rewriting the code in a compiled language such as `C++` could also allow for improved performance.

7 Acknowledgments

This project was carried out together with Ben Bullinger and Francesco Conoscenti.

We closely followed the derivations and explanations in Victor Drouin-Touchette's notes *The Kosterlitz-Thouless Phase Transition: An Introduction for the Intrepid Student* (2022) throughout this work [2].

I used OpenAI's ChatGPT (May 2025 version) to assist with grammar correction and improving the clarity of explanations in this report.

Notes

During this project, I contributed to the following tasks:

- Implemented the spin–spin correlation function $g(r)$.
- Extracted the decay exponent η and correlation length ξ from $g(r)$ using algebraic and exponential fits.
- Determined T_{BKT} from the temperature dependence of $\eta(T)$ and $\xi(T)$.
- Performed jackknife resampling for c_v, χ, U, ω_{v} and $g(r)$.
- Applied error propagation for $T_{\mathrm{BKT}}(L)$ estimates based on spin stiffness and η.

References

[1] Bertrand Berche, Ana Farinas-Sanchez, and Ricardo Paredes. Correlations in the low-temperature phase of the two-dimensional xy model. *EPL (Europhysics Letters)*, 60, 08 2002.

[2] Victor Drouin-Touchette. The kosterlitz-thouless phase transition: an introduction for the intrepid student, 2022.

[3] Mehran Kardar. *Statistical Physics of Fields*. Cambridge University Press, 2007.

[4] J M Kosterlitz. The critical properties of the two-dimensional xy model. *Journal of Physics C: Solid State Physics*, 7(6):1046, mar 1974.

[5] Siu Kwan Lam, Antoine Pitrou, and Stanley Seibert. Numba: A LLVM-based Python JIT compiler. *Proceedings of the Second Workshop on the LLVM Compiler Infrastructure in HPC*, pages 1–6, 2015.

[6] I. Maccari, N. Defenu, L. Benfatto, C. Castellani, and T. Enss. Interplay of spin waves and vortices in the two-dimensional xy model at small vortex-core energy. *Phys. Rev. B*, 102:104505, Sep 2020.

[7] N. D. Mermin and H. Wagner. Absence of ferromagnetism or antiferromagnetism in one- or two-dimensional isotropic heisenberg models. *Phys. Rev. Lett.*, 17:1133–1136, Nov 1966.

[8] David Mukamel. The 2d coulomb gas and the kosterlitz–thouless transition. https://www.weizmann.ac.il/complex/mukamel/sites/complex.mukamel/files/uploads/2013-culombgas2d.pdf, 2013. Lecture notes, Weizmann Institute of Science.

[9] David R. Nelson and J. Michael Kosterlitz. Universal jump in the superfluid density of two-dimensional superfluids. *Phys. Rev. Lett.*, 39(19):1201–1205, 1977.

[10] Peter Olsson. Monte carlo analysis of the two-dimensional xy model. ii. comparison with the kosterlitz renormalization-group equations. *Phys. Rev. B*, 52:4526–4535, Aug 1995.

[11] Kari Rummukainen. Monte carlo simulation methods – lecture 5: Error analysis: Jackknife & bootstrap. https://www.mv.helsinki.fi/home/rummukai/lectures/montecarlo_oulu/lectures/mc_notes5.pdf, n.d. Accessed: 2025-05-15.

[12] University of Washington. Propagation of errors—basic rules. https://courses.washington.edu/phys431/propagation_errors_UCh.pdf, 2001. Accessed: 2025-05-15.

[13] Wikipedia contributors. Jackknife resampling — Wikipedia, the free encyclopedia, 2024. Accessed: 2025-05-15.